Targeting *EZH2* oncogenic splicing: decoding the regulatory network and antisense correction

Md Rafikul Islam, Preeti Nagar, Naomi McNaughton, et al.

Genes Dev. published online August 3, 2026
Access the most recent version at doi:10.1101/gad.353628.126

Targeting *EZH2* oncogenic splicing: decoding the regulatory network and antisense correction

Md Rafikul Islam,[1,2,6] Preeti Nagar,[1,2,6] Naomi McNaughton,[1] Shabiha Afroj Heeamoni,[1] Md Mahbub Hasan,[1] Shila Kandel,[1] Israt Jahan Mukta,[1] Panagiotis Tsakiroglou,[3] William Brian Dalton,[3] Omar Abdel-Wahab,[4] Adrian R. Krainer,[5] and Mohammad Alinoor Rahman[1,2]

[1]Department of Biochemistry and Molecular Biology, University of Arkansas for Medical Sciences, Little Rock, Arkansas 72205, USA; [2]Winthrop P. Rockefeller Cancer Institute, University of Arkansas for Medical Sciences, Little Rock, Arkansas 72205, USA; [3]Division of Hematologic Malignancies and Bone Marrow Transplantation, Department of Oncology, Sidney Kimmel Comprehensive Cancer Center, Johns Hopkins University School of Medicine, Baltimore, Maryland 21231, USA; [4]Molecular Pharmacology Program, Sloan Kettering Institute, Memorial Sloan Kettering Cancer Center (MSK), New York, New York 10065, USA; [5]Cold Spring Harbor Laboratory, Cold Spring Harbor, New York 11724, USA

Recurrent mutations in splicing factors (SFs) have been established as crucial drivers of tumorigenesis in several types of blood cancer and are also common in a variety of solid tumors. Mutations change the RNA-binding preferences of SFs, promote global splicing alterations, and often generate erroneous mRNAs that are then degraded by nonsense-mediated mRNA decay (NMD). Consequently, several critical genes linked to hematopoiesis are dysregulated, leading to blood cancer. Although the field has progressed considerably in identifying aberrant genes and affected pathways, effective therapies have not yet emerged. To address this key gap, we instigated a gene-specific targeted strategy by unlocking the regulatory network. As a proof of concept, we scrutinized a tumor suppressor gene, *EZH2*, which is a bona fide target in SRSF2 mutated cancer. We precisely defined splicing *cis*-elements in *EZH2* transcripts and illustrated the dynamic choreography of regulatory proteins in the entire splicing and NMD catalytic pathways. We then designed antisense oligonucleotides (ASOs) targeting important regulatory sites. Our lead ASO successfully corrects aberrant splicing and NMD, restores the expression and function of EZH2, and partially rescues hematopoietic defects and cellular properties. Our study demonstrates that ASO pharmacology is an actionable strategy for clinical development, challenging the existing paradigms in SF mutated cancers.

[*Keywords*: antisense oligonucleotide therapy; cancer; gene expression; nonsense-mediated mRNA decay; RNA splicing]

Supplemental material is available for this article.

Received January 1, 2026; revised version accepted April 30, 2026.

Recurrent oncogenic heterozygous mutations in RNA splicing factors are frequent in patients with myelodysplastic syndromes (MDS), and occur in clonal hematopoiesis, acute myeloid leukemia (AML), chronic lymphocytic leukemia (CLL), and a variety of solid tumors (Yoshida et al. 2011; Bradley and Anczuków 2023). The most frequent mutations occur in SF3B1, SRSF2, U2AF1, or ZRSR2 in highly restricted residues (except for ZRSR2). Since the discovery of splicing factor mutations, considerable progress has been made in identifying aberrantly spliced mRNAs, thanks to advancements in next-generation sequencing. Mutations in splicing factors usually change their RNA-binding properties and cause genome-wide splicing alterations (Bradley and Anczuków 2023; Zhang et al. 2024). Some of these splicing changes are directly associated with tumorigenesis (cancer driver), while others are not linked with cancer (nondriver) (Zhang et al. 2015; Rahman et al. 2020a; Bradley and Anczuków 2023). Cancer driver aberrant splicing events serve as important biomarkers and potential therapeutic targets.

Although initially it was predicted that mutations in different splicing factors may have common downstream effects (Yoshida et al. 2011), research in the past decade revealed that different mutations have different downstream targets. This appeared to be a critical roadblock to developing a generalized therapeutic approach to treat all splicing factor mutated cancer patients commonly. Indeed, a generalized strategy to therapeutically target RNA splicing in cancers remains mostly ineffective to date (Lee

[6]**These authors contributed equally to this work.**
Corresponding author: marahman@uams.edu
Article published online ahead of print. Article and publication date are online at http://www.genesdev.org/cgi/doi/10.1101/gad.353628.126. Freely available online through the *Genes & Development* Open Access option.

and Abdel-Wahab 2016; Seiler et al. 2018; Liu et al. 2024). Although there has been noteworthy progress in the last 5 years, with several new US FDA-approved therapies for AML (unrelated to splicing), the 5 year survival for most AML patients remains <20%, and there are limited effective therapies for MDS (Daver et al. 2020; Kim et al. 2025). Thus, there remains an unmet medical need to develop more effective targeted therapeutic approaches, based on a precise understanding of molecular regulation.

Eukaryotic gene expression involves a series of highly regulated and interconnected pathways and surveillance systems to ensure its fidelity. Nonsense-mediated mRNA decay (NMD) is a posttranscriptional surveillance mechanism to selectively identify and degrade erroneous mRNAs comprising a premature termination codon (PTC). PTCs are usually generated by nonsense or frameshift mutations. Alternative RNA splicing (AS) can also generate erroneous mRNAs with a premature termination codon (PTC), which are degraded by NMD. This is termed as splicing-coupled-NMD or shortly AS-NMD. Studies in recent decades identified AS-NMD as a crucial regulator of gene expression (Colombo et al. 2017; Rahman et al. 2020b; Nagar et al. 2023). Tumor cells often differentially exploit AS-NMD for their survival benefit, such as inducing AS-NMD to downregulate tumor suppressor(s) or inhibiting AS-NMD to stabilize oncoprotein(s) (Popp and Maquat 2014, 2018; Park et al. 2019; Rahman et al. 2020b; Nagar et al. 2023). AS-NMD has been identified as a common mediator of tumorigenesis in all splicing factor mutated cancers (Graubert et al. 2011; Darman et al. 2015; Ilagan et al. 2015; Kim et al. 2015; Inoue et al. 2019; Yoshimi et al. 2019; Rahman et al. 2020b).

Understanding the molecular mechanisms and consequences of individual splicing-factor mutations is crucial for developing novel targeted splicing-based therapies. Here, we focus on SRSF2, which is a member of the serine-arginine-rich (SR) protein family. SR proteins are reported to play important roles in both constitutive and alternative splicing, NMD, mRNA transport, transcriptional and translational regulations (Zhang et al. 2015; Rahman et al. 2020a; Bradley and Anczuków 2023). Here, we developed experimental approaches to dissect the detailed molecular mechanisms of a bona fide cancer driver AS-NMD event in *EZH2* in SRSF2 mutated cancer. Exploiting minigene reporters, model cell lines, and biochemical and functional approaches, we dissected the underlying mechanisms of aberrant inclusion of a poison exon in *EZH2*. We defined critical binding motifs of mutant SRSF2 in *EZH2* and characterized transcript-specific interacting protein assembly in the entire RNA processing pathway from splicing to NMD. We then developed antisense oligonucleotides (ASO) that efficiently corrected the aberrant splicing and restored the expression of EZH2 protein, evading AS-NMD. Furthermore, the ASO enhanced histone methylation (H3K27me3), improved cell viability, modulated cell cycle kinetics, reduced apoptosis, and showed promising effects in rescuing defective hematopoiesis. Our approach is promising and will pave the way for future targeted therapeutic development in splicing factor mutated cancer.

Results

Aberrant splicing of the EZH2 *poison exon is a crucial tumorigenic target in SRSF2 mutated blood cancer*

We previously investigated AML patient RNA-sequencing data set from the Cancer Genome Atlas (TCGA-LAML) for SRSF2 Pro95 mutant versus SRSF2 wild-type (Rahman et al. 2020b). We have reanalyzed the data to detect a potential tumorigenic target to push our study forward toward therapeutic development dependent on mechanistic insights. Among 843 differential splicing events, about half of the events are cassette exon splicing (ES), and the remaining half include alternative splice site selection (ASS) and intron retention (IR) events in similar proportions (Supplemental Fig. S1A). One striking observation is that 135 mRNA isoforms (~16%) among these events are NMD targets (AS-NMD), which are distributed among all types of splicing events, but with higher representation in the ES group (Fig. 1A; Supplemental Fig. S1B). Aberrant AS-NMD has also been identified as a major mechanism of tumorigenesis in SF3B1 and U2AF1 mutated patients (Darman et al. 2015; Ilagan et al. 2015; Inoue et al. 2019). Analysis of cassette exons ($SRSF2^{Mut}$ vs. $SRSF2^{WT}$) to quantify enriched motifs using the MEME (Bailey et al. 2009) shows preferential enrichment of (G/C)C(A/T)G motifs in promoted exons, and GG(A/T)G motifs in repressed exons (Fig. 1B,C). These consensus motifs retrieved from RNA-sequencing are consistent with previous studies, including samples from cancer patients, animal models, and cell lines (Kim et al. 2015; Komeno et al. 2015; Zhang et al. 2015). A recent study determined motif enrichment from in vivo HITS-CLIP (high-throughput sequencing of RNA isolated by crosslinking immunoprecipitation) and identified similar motifs (Liang et al. 2018). Taken together, these analyses show that CCWG is the consensus motif preferred for $SRSF2^{Mut}$ (W=A/T), whereas GGWG is the motif for $SRSF2^{WT}$. The change in RNA binding preferences causes a gain of function in $SRSF2^{Mut}$ and triggers aberrant splicing of a set of target genes, some of which are strongly associated with defective hematopoietic differentiation (Kim et al. 2015; Zhang et al. 2015; Yoshimi et al. 2019). Among consistently identified genes in multiple studies, a few validated and noteworthy cancer-relevant aberrant splicing targets include *EZH2, INTS3, and CLK3* (Kim et al. 2015, 2025; Yoshimi et al. 2019; Rahman et al. 2020b). *EZH2* encodes the enhancer of zeste homolog 2 protein (EZH2), which catalyzes methylation of histone H3 at lysine 27 (H3K27me3), and therefore functions in chromatin remodeling (Fig. 1D; Tan et al. 2014). EZH2, as a component of the polycomb repressive complex 2 (PRC2), was reported to suppress gene expression and regulate cell fate (Tan et al. 2014). A poison exon (PE) in *EZH2* is exclusively included in $SRSF2^{Mut}$ patients (Fig. 1E), which generates a PTC and triggers the degradation of *EZH2* transcripts by AS-NMD (Kim et al. 2015; Yoshimi et al. 2019; Rahman et al. 2020b). Downregulation of EZH2 protein

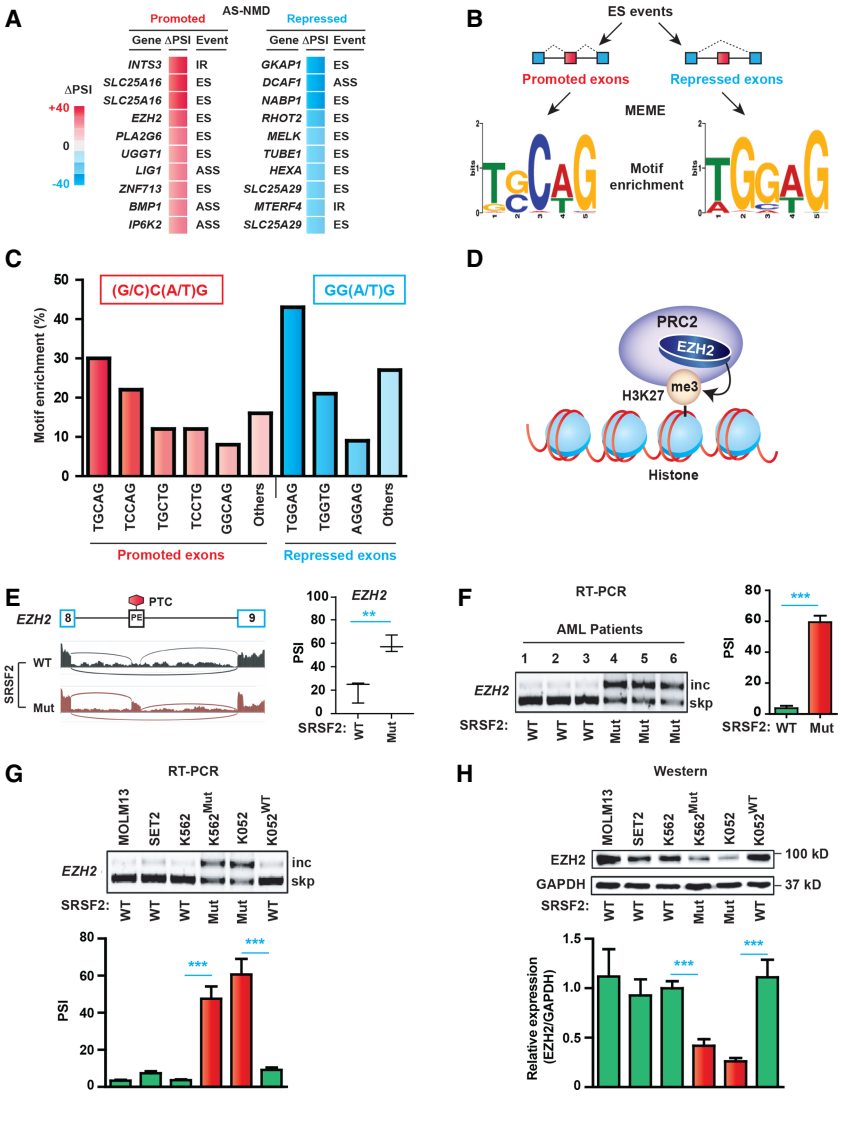

Figure 1. Tumorigenic aberrant splicing targets in SRSF2 mutated blood cancer. (*A*) The top 10 AS-NMD events are listed in promoted and repressed alternative splicing events, respectively. ΔPSI: changes in percent spliced-in ($SRSF2^{Mut}$ vs. $SRSF2^{WT}$). Multiple AS-NMD events are observed for the same gene on several occasions. (*B*) Schematic of motif enrichment analysis in promoted or repressed cassette exons ($SRSF2^{Mut}$ vs. $SRSF2^{WT}$) using MEME. (*C*) Proportion of different motifs enriched in promoted or repressed cassette exons. Consensus sequences of enriched motifs are shown above in enclosed boxes. (*D*) Schematic of EZH2 protein function in histone methylation (H3K27me3) and chromatin regulation. (PRC2) Polycomb repressing complex. (*E*, *left*) Representative Sashimi plots showing *EZH2* poison exon inclusion in acute myeloid leukemia (AML) samples from the genotypes indicated. (*Right*) Quantification of *EZH2* poison exon inclusion as percent spliced-in (PSI) in AML samples from the genotypes indicated (mean ± SD, $n = 3$). (**) $P < 0.01$, *t*-test. (*F*, *left*) RT-PCR gel showing *EZH2* poison exon inclusion (inc) and skipping (skp) in an independent set of AML samples with $SRSF2^{WT}$ and $SRSF2^{Mut}$. (*Right*) Quantification of *EZH2* poison exon inclusion as PSI is shown by a bar graph (mean ± SD, $n = 3$). (***) $P < 0.001$, *t*-test. (*G*) Representative RT-PCR gel showing *EZH2* poison exon inclusion and skipping in different human leukemia cell lines from the genotypes indicated *below*. Quantification of *EZH2* poison exon inclusion as PSI is shown by a bar graph *below* the gel (mean ± SD, $n = 3$). (***) $P < 0.001$, *t*-test. (*H*) Western blotting of EZH2 protein expression in different human leukemia cell lines from *G*. GAPDH was used as an internal control. Relative quantification of EZH2 protein expression (EZH2/GAPDH) is shown by a bar graph below the gel (mean ± SD, $n = 3$). (***) $P < 0.001$, *t*-test.

expression through AS-NMD consequently leads to defective hematopoietic differentiation in $SRSF2^{Mut}$ cancer (Kim et al. 2015; Yoshimi et al. 2019; Rahman et al. 2020b).

We confirmed aberrant poison exon inclusion in *EZH2* in an independent pool of AML patient RNA samples with $SRSF2^{Mut}$ compared to $SRSF2^{WT}$ (Fig. 1F). This was also consistently shown in several other studies (Kim et al. 2015; Masaki et al. 2019; Yoshimi et al. 2019; Grimm et al. 2021). We analyzed several cell lines originating from leukemia patients, with inherently harboring wild-type ($SRSF2^{WT/WT}$) or heterozygous mutant ($SRSF2^{Mut/WT}$) genotypes. These included MOLM13 ($SRSF2^{WT/WT}$), SET2 ($SRSF2^{WT/WT}$), K562 ($SRSF2^{WT/WT}$), and K052 ($SRSF2^{P95H/WT}$), where SRSF2 genotypes are mentioned in brackets. RT-PCR and western blotting showed exclusive poison exon inclusion into *EZH2* mRNA and concomitant protein downregulation only in K052 ($SRSF2^{P95H/WT}$) but not in the other cell lines (Fig. 1G, H). We additionally included an engineered K562 cell line, termed $K562^{Mut}$, in which the *SRSF2* P95H mutation was introduced into the endogenous locus as a heterozygous mutation ($SRSF2^{P95H/WT}$). As expected, $K562^{Mut}$ showed enhanced poison exon inclusion into *EZH2* mRNA compared to K562 (Fig. 1G). This was also reflected at the protein level, with downregulation of EZH2 protein expression (Fig. 1H). Finally, we included another engineered K052 cell line, termed $K052^{WT}$, in which the *SRSF2* P95H mutation was reverted to *SRSF2* WT in the endogenous gene locus ($SRSF2^{WT/WT}$). Indeed, $K052^{WT}$ showed a reduction of poison exon inclusion into *EZH2* mRNA, and upregulated EZH2 protein expression compared to K052 ($SRSF2^{P95H/WT}$) (Fig. 1G,H). These rigorous experimental results clearly confirmed the $SRSF2^{Mut}$-dependent poison exon inclusion activity in *EZH2*. We therefore selected *EZH2* as a bona fide target for downstream mechanistic analyses aimed at developing a potential therapeutic strategy.

Experimental models to characterize mechanisms of regulation by mutant SRSF2

To study the precise mechanisms of action that link mutant SRSF2 to tumorigenesis, we engineered K562 cells and stably integrated a doxycycline (DOX)-inducible construct to express cDNA encoding FLAG-tagged SRSF2^{WT} or SRSF2^{P95H} conditionally (Fig. 2A). These cell lines are termed K562(DOX)SRSF2^{WT} and K562(DOX)SRSF2^{P95H}, respectively. We also engineered a nonhematopoietic HeLa cell line expressing DOX-inducible FLAG-tagged SRSF2^{WT} or SRSF2^{P95H} to examine any tissue-specific regulation (Supplemental Fig. S2). These cell lines allow the study of SRSF2^{WT}- or SRSF2^{P95H}-specific regulatory mechanisms in splicing and NMD, following DOX-inducible expression. Although SRSF2 is involved in multiple biological pathways, conditional expression over a short period is intended to exclude indirect or feedback effects from other pathways, and/or long-term cellular effects exerted by the mutant factor.

EZH2 *PE splicing is regulated by the presence or absence of a specific exonic splicing enhancer*

Inclusion of an alternative exon is usually regulated by an exonic splicing enhancer (ESE), and often by an intronic splicing enhancer (ISE) (Black 2003; Licatalosi and Darnell 2006). As noted earlier, Pro95 mutations in SRSF2 change its RNA-binding preference from GGWG to CCWG. Tabulating these motifs revealed that *EZH2* poison exon harbors three preferred binding motifs (CCWG) of SRSF2^{Mut}, but no binding motif (GGWG) of SRSF2^{WT} (Supplemental Fig. S3). Splicing regulatory ESE in an alternative exon

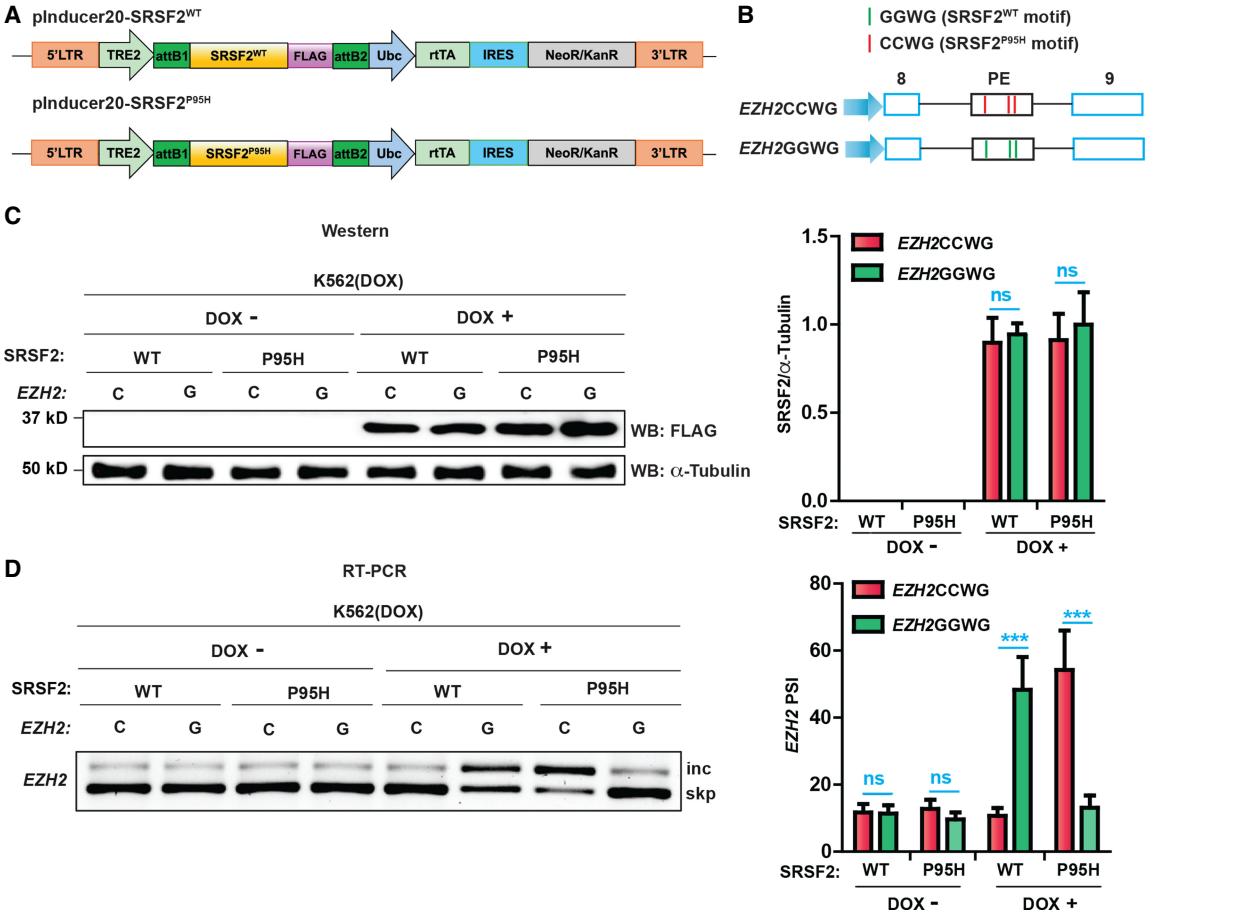

Figure 2. Alternative splicing of the *EZH2* poison exon is regulated by the presence or absence of specific ESE elements. (*A*) Diagram of DOX-inducible FLAG-tagged cDNA constructs to generate K562(DOX) stable cell lines expressing either SRSF2^{WT} or SRSF2^{P95H} in the presence of DOX. (*B*) Diagram (not to scale) of *EZH2* minigene reporters harboring different combinations of SRSF2 (Mut or WT) motifs within the poison exon. *EZH2*CCWG (C) contains native gene sequences with three SRSF2^{Mut}-binding motifs (CCWG), whereas *EZH2*GGWG (G) contains three SRSF2^{WT}-binding motifs (GGWG) replacing CCWG motifs (W = A/T). (*C*, *left*) Western blotting (WB) of the indicated K562(DOX) cells cotransfected with the indicated *EZH2* minigene reporters with the indicated antibodies. α-Tubulin was used as an internal control. (*Right*) Quantification of SRSF2 (WT or P95H) protein expression (normalized against α-tubulin) is shown by a bar graph (mean ± SD, $n = 3$). (ns) Not significant, *t*-test. (*D*, *left*) Representative RT-PCR gel showing *EZH2* minigene reporter-specific poison exon inclusion (inc) and skipping (skp) in the indicated K562(DOX) cells cotransfected with the indicated *EZH2* minigene reporters. (*Right*) Quantification of *EZH2* minigene reporter-specific poison exon inclusion as percent spliced-in (PSI) is shown by a bar graph (mean ± SD, $n = 3$). (***) $P < 0.001$, (ns) not significant, *t*-test.

often harbors multiple *cis*-elements or binding motifs, and these motifs coordinately regulate the binding of splicing factor(s) and subsequent splicing modulation (Nasrin et al. 2014, 2025; Feng et al. 2019). To systematically identify splicing regulatory elements in *EZH2* poison exon ESE, we employed an *EZH2* minigene reporter (*EZH2*CCWG) with native gene sequences (Kim et al. 2015), consisting of three binding motifs of $SRSF2^{Mut}$ in the PE (Fig. 2B). We also employed another modified minigene (*EZH2*GGWG), where all of the three binding motifs of mutant SRSF2 were changed to preferred motifs for $SRSF2^{WT}$ (Fig. 2B). We then transfected these minigene reporters into DOX-inducible K562 cells for splicing analyses. We first confirmed the comparable levels of expression of $SRSF2^{WT}$ and $SRSF2^{Mut}$ upon DOX treatment by western blotting (Fig. 2C). We then performed RT-PCR to study minigene reporter-specific splicing profiles by employing a reporter-specific primer during cDNA synthesis. In the absence of DOX, we found no changes in *EZH2* PE splicing between $SRSF2^{P95H}$ and $SRSF2^{WT}$ expressing cells (Fig. 2D). To our expectation, DOX treatment could clearly enhance PE inclusion in *EZH2*CCWG reporter in $SRSF2^{P95H}$ expressing cells, but not in $SRSF2^{WT}$ expressing cells (Fig. 2D). These data clearly demonstrated CCWG-dependent ESE-activity of $SRSF2^{Mut}$ in native *EZH2* reporter (*EZH2*CCWG). Surprisingly, DOX treatment could also enhance PE inclusion in the *EZH2*GGWG reporter in $SRSF2^{WT}$ expressing cells, but not in $SRSF2^{P95H}$ expressing cells. These data suggest that the lack of the $SRSF2^{WT}$-binding motif in *EZH2* PE disables exon inclusion in normal cells expressing $SRSF2^{WT}$, whereas the presence of the $SRSF2^{Mut}$ motif promotes *EZH2* PE inclusion in SRSF2 mutated blood cancer cells. We also performed the experiment in DOX-inducible HeLa cells. Our data in HeLa cells (Supplemental Fig. S2A,B) showed consistent results with that of K562 cells (Fig. 2), thereby ruling out any tissue-specific differential regulation. Taken together, we can conclude that the presence or absence of preferred RNA-binding motif (s) in the *EZH2* PE ESE can dictate the splicing consequences promoted by $SRSF2^{Mut}$ or $SRSF2^{WT}$.

Systematic identification of the crucial functional motif in the ESE of EZH2 *PE*

Among multiple motifs in a splicing regulatory ESE, a specific motif often plays a crucial role in cooperative binding or stable association of splicing factor(s) with RNA (Nasrin et al. 2014, 2025; Feng et al. 2019). Therefore, identification of a crucial functional motif could provide the opportunity to develop a splicing modulation strategy by targeting a specific region of RNA either by generating steric hindrance, affecting RNA structure, or interfering with the binding of splicing factor(s). To this end, we wanted to define the contribution of individual binding motifs on $SRSF2^{Mut}$-mediated *EZH2* PE inclusion. We employed systematic inactivation of individual binding motifs in the minigene reporter, followed by analyzing splicing consequences. To inactivate the $SRSF2^{Mut}$ binding motif, we changed the CCWG motif to the AAWG motif, which is preferred neither by $SRSF2^{Mut}$ nor by $SRSF2^{WT}$, as we showed previously (Rahman et al. 2020b). Note that among the three binding motifs of $SRSF2^{Mut}$ in the *EZH2* poison exon, motifs 2 and 3 overlap (Supplemental Fig. S3). Therefore, we employed three mutant versions of *EZH2* reporter: *EZH2*MUT1 harbors inactivated motif 1; *EZH2*MUT2 harbors inactivated motifs 2 and 3; and *EZH2*MUT3 harbors inactivated motifs 1, 2, and 3 (Fig. 3A). We then performed minigene reporter-specific splicing assay using RT-PCR. In K562(DOX) $SRSF2^{WT}$ or K562(DOX)$SRSF2^{P95H}$, in the absence of DOX, we observed no considerable changes in *EZH2* PE inclusion (Fig. 3B). However, upon DOX treatment in K562(DOX)$SRSF2^{P95H}$, we found significant loss of *EZH2* PE inclusion in *EZH2*MUT1 and *EZH2*MUT3, compared to *EZH2*CCWG (native) (Fig. 3B). Note that motif 1 was inactivated in both *EZH2*MUT1 and *EZH2*-MUT3. Therefore, the results highlight the importance of motif 1 for $SRSF2^{Mut}$ and also suggest that motifs 2 and 3 are not enough in the absence of motif 1. In contrast, we observed a slight loss of *EZH2* PE inclusion in *EZH2*-MUT2 compared to *EZH2*CCWG (native) (Fig. 3B). This observation indicates that motif 1 is functional even in the absence of motifs 2 and 3; however, motifs 2 and 3 have additive effects, which may function in cooperation with motif 1. It is important to note that the above changes were not evident upon DOX induction in K562(DOX) $SRSF2^{WT}$, as expected due to the lack of $SRSF2^{WT}$ binding motif (Fig. 3B). Taken together, these data clearly suggest the essentiality and critical importance of motif 1 in regulating $SRSF2^{Mut}$-mediated *EZH2* PE inclusion.

MS2-mediated tethering of SRSF2 to a specific binding motif in EZH2 *PE is sufficient to promote exon inclusion*

Having identified the functional motifs for ESE activity in *EZH2* poison exon, we next sought to identify whether site-specific tethering of $SRSF2^{Mut}$ to the motif site could reproduce ESE-activity (Fig. 3C). To this end, we generated two additional versions of *EZH2* reporter: *EZH2*MUT4, where we replaced motif 1 with the MS2 coat protein-binding hairpin sequences (Rahman et al. 2020b), and inactivated both motifs 2 and 3 to AAWG; and *EZH2*MUT5, where we replaced both motifs 2 and 3 with the MS2 coat protein-binding hairpin sequences, and inactivated motif 1 to AAWG (Fig. 3C). These reporters, therefore, allow to evaluate the effect of MS2-mediated artificial tethering of SRSF2 for only one site at a time. We generated MS2-tagged-T7-$SRSF2^{WT}$ (MS2-$SRSF2^{WT}$) and MS2-tagged-T7-$SRSF2^{Mut}$ (MS2-$SRSF2^{P95H}$) cDNA constructs and confirmed their comparable expression in K562 (Fig. 3D). We then simultaneously transfected K562 cells with an *EZH2* reporter and MS2-tagged SRSF2 cDNA (WT or Mut) and performed minigene reporter-specific splicing assay using RT-PCR. Recruitment of MS2-$SRSF2^{Mut}$ to only motif 1 site (*EZH2*MUT4) significantly enhanced exon inclusion activity (Fig. 3E). In contrast, recruitment of MS2-$SRSF2^{Mut}$ to the site spanning motifs 2 and 3 (*EZH2*MUT5) also enhanced exon inclusion activity, but to a lesser extent than only motif 1 site

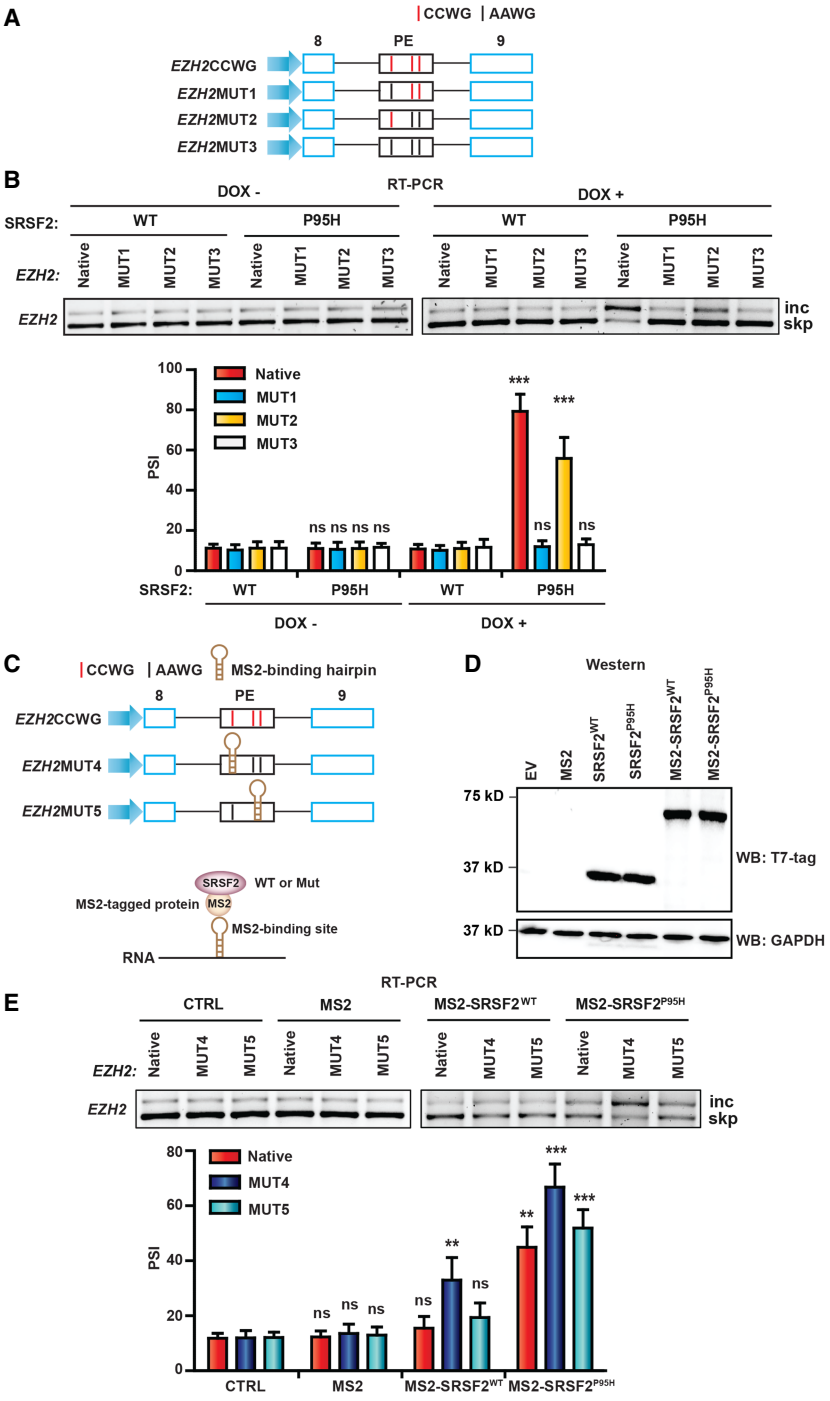

Figure 3. Decoding crucial ESE motif in the *EZH2* poison exon regulated by SRSF2^{Mut}. (*A*) Diagram (not to scale) of *EZH2*CCWG (native) and three mutant minigene reporters. *EZH2*CCWG (native) contains native gene sequences with three SRSF2^{Mut}-binding motifs (CCWG): motifs 1, 2, and 3, respectively (W = A/T). These CCWG motifs were mutated to AAWG to inactivate the binding of SRSF2^{Mut} in different combinations in mutant reporters. (*B*, *top*) Representative RT-PCR gels showing *EZH2* minigene reporter-specific poison exon inclusion (inc) and skipping (skp) in K562 (DOX)SRSF2^{WT} or K562(DOX)SRSF2^{P95H} cells cotransfected with the indicated *EZH2* minigene reporters. (*Bottom*) Quantification of *EZH2* minigene reporter-specific poison exon inclusion as percent spliced-in (PSI) is shown by a bar graph (mean ± SD, $n = 3$). (***) $P < 0.001$, (ns) not significant, *t*-test, SRSF2^{P95H} versus SRSF2^{WT}. (*C*, *top*) Diagram (not to scale) of *EZH2*CCWG (native) and two mutant minigene reporters. In *EZH2*MUT4, motif 1 was replaced by the MS2 coat protein-binding hairpin, and motifs 2 and 3 were inactivated to AAWG. In *EZH2*MUT5, motifs 2 and 3 were replaced by the MS2 coat protein-binding hairpin, and motif 1 was inactivated to AAWG. (*Bottom*) Schematic of targeted recruitment of MS2-tagged SRSF2 (WT or Mut) to a specific site of a transcript harboring the MS2 coat protein-binding hairpin. (*D*) Western blotting (WB) of K562 cells transfected with the indicated cDNA vectors. Note that the empty vector (CTRL) and only MS2 (MS2) have no T7-tag. (*E*, *top*) Representative RT-PCR gels showing *EZH2* minigene reporter-specific poison exon inclusion (inc) and skipping (skp) in K562 cells cotransfected with the indicated *EZH2* minigene reporters and cDNAs. (*Bottom*) Quantification of *EZH2* minigene reporter-specific poison exon inclusion as percent spliced-in (PSI) is shown by a bar graph (mean ± SD, $n = 3$). (**) $P < 0.01$, (***) $P < 0.001$, (ns) not significant, *t*-test, compared to corresponding CTRL.

(*EZH2*MUT4) (Fig. 3E). We also observed exon inclusion activity of MS2-SRSF2^{Mut} in *EZH2*CCWG (native) reporter without MS2 hairpin, because MS2-SRSF2^{Mut} can still bind to CCWG motifs through its SRSF2^{Mut} part of the fusion protein. Note that MS2 alone showed no effects in any of the reporters, ruling out any possible experimental artifacts promoted by the MS2-tag. Interestingly, recruitment of MS2-SRSF2^{WT} to only motif 1 site also promoted exon inclusion activity, because MS2-SRSF2^{WT} was able to bind the PE through MS2 hairpin even in the absence of GGWG motif (Fig. 3E). These data again support that the presence or absence of preferred RNA-binding motif (s) in an ESE of a target exon could dictate the splicing consequences promoted by SRSF2^{Mut} or SRSF2^{WT}.

Mutant SRSF2 enhances the deposition of several key spliceosome components and NMD-associated factors to augment AS-NMD of EZH2

AS-NMD is regulated at multiple levels of RNA metabolism, including splicing of pre-mRNA, mRNA surveillance to selectively identify erroneous mRNAs with a

premature termination codon, mRNA transport, and rapid degradation of faulty mRNAs. These metabolisms are choreographed with dynamic interactions between RNA and ribonucleoproteins (RNPs) at individual stages (Lykke-Andersen and Jensen 2015; Woodward et al. 2017; Kurosaki et al. 2019; Nagar et al. 2023). To identify how assembly of RNPs is regulated by SRSF2^{Mut} in *EZH2* transcripts, we exploited the MS2 coat protein-mediated RNPs pull-down system that we described before (Rahman et al. 2020b). We constructed two additional modified versions of *EZH2 reporters*, *EZH2*CCWG-3×MS2, and *EZH2*AAWG-3xMS2, where we introduced three MS2-binding hairpin sequences at the 3′ end of the reporters (Fig. 4A). Transcripts (both pre-mRNA and mRNA) originating from these minigenes will generate MS2-binding hairpins. After transfecting these reporters in K562 (DOX)SRSF2^{WT} or K562(DOX)SRSF2^{P95H} cells, MS2 hairpins-containing transcripts and associated RNPs can be selectively captured using a recombinant MS2-tagged maltose binding protein (MS2-MBP) and amylose resin

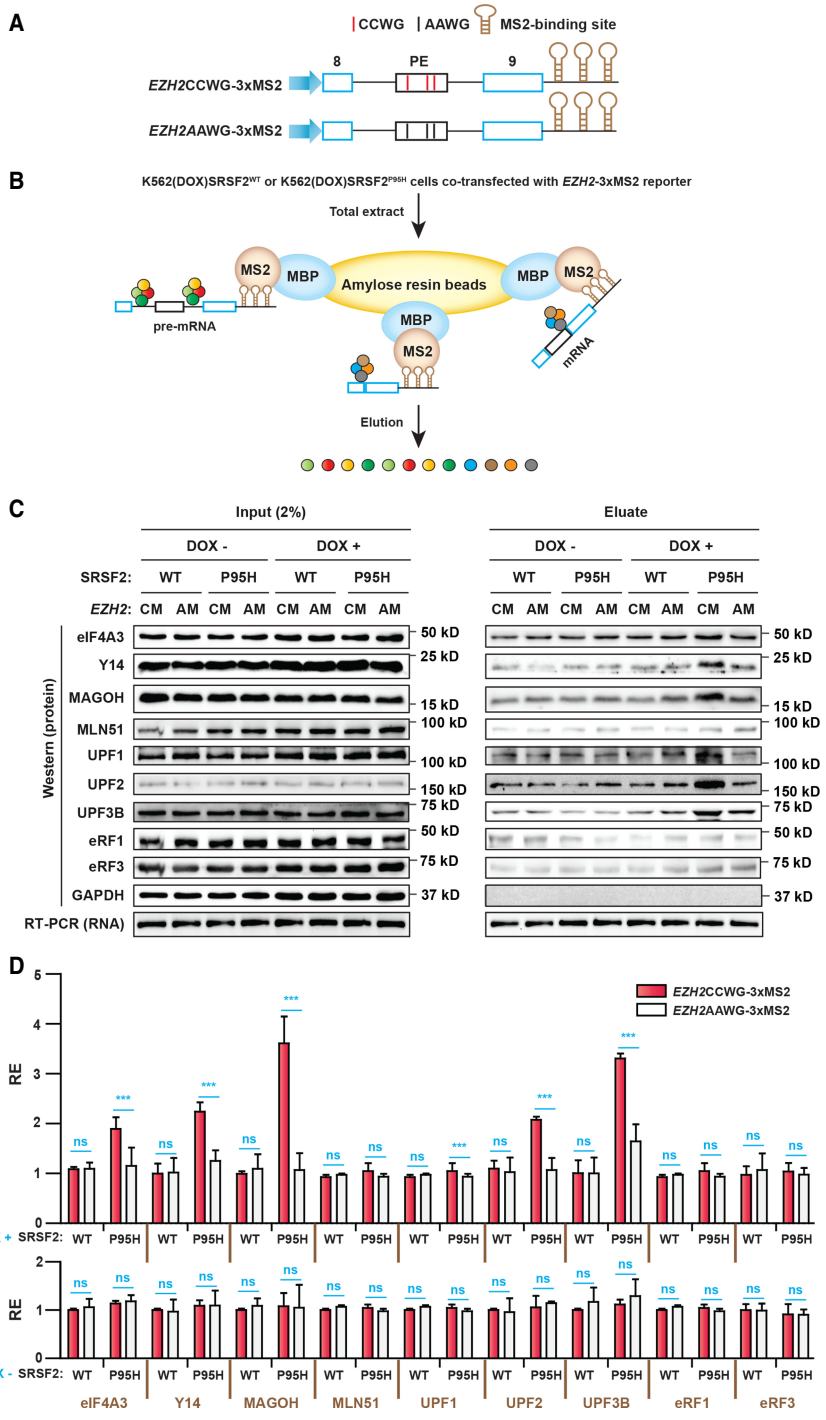

Figure 4. Purification of ribonucleoproteins (RNPs) from *EZH2* minigene reporter-specific transcripts. (*A*) Diagram (not to scale) of *EZH2*-3xMS2 minigene reporters harboring three MS2 coat protein-binding hairpin sequences downstream from exon 9. *EZH2*CCWG-3xMS2 (CM) contains native gene sequences with three SRSF2^{Mut}-binding motifs (CCWG). *EZH2*AAWG-3xMS2 (AM) contains three AAWG motifs (not a binding site for SRSF2^{Mut} or SRSF2^{WT}) replacing respective CCWG motifs. (*B*) Schematics of MS2-mediated RNPs purification from *EZH2*-3xMS2-specific transcripts (both pre-mRNA and mRNA). Recombinant MS2-tagged maltose-binding protein (MS2-MBP) and amylose resin beads were used to purify the MS2 hairpin-containing transcripts originating from *EZH2*-3xMS2 reporter transfected into K562(DOX)SRSF^{WT} or K562(DOX) SRSF2^{P95H} cells. (*C*) Representative western blotting and RT-PCR of input or purified RNA and RNPs from the indicated K562 (DOX) cells cotransfected with the indicated reporters. (*D*) Quantification of the relative enrichment (RE) of EJC components and NMD factors into *EZH2*CCWG-3xMS2 transcripts compared to *EZH2*AAWG-3xMS2 transcripts, normalized against RNA purified from transfected K562(DOX) cells with the indicated genotypes in the presence or absence of DOX (mean ± SD, $n = 3$). (***) $P < 0.001$, (ns) not significant, *t*-test.

beads (Fig. 4B). Purified RNPs can then be resolved and quantified by western blotting. We performed the experiments and quantified the assembly of major spliceosome components and NMD-associated proteins, such as exon junction complex (EJC) and NMD factors, into *EZH2* transcripts (Fig. 4C,D; Supplemental Fig. S4A,B). Our results showed that SRSF2^{P95H} expression (upon DOX treatment) enhances the assembly of several key spliceosome components in *EZH2*CCWG-3xMS2 transcripts compared to *EZH2*AAWG-3xMS2, including U1snRNP 70K (U1-70K), U1 snRNP A (U1A), U1 snRNP C (U1C), U2AF65, and U2AF35 but not SF3B1 (Supplemental Fig. S4A,B). Similarly, SRSF2^{P95H} expression enhances deposition of several EJC components, such as eIF4A3, Y14, MAGOH, but not MLN51 (Fig. 4C,D). Among NMD factors, SRSF2^{P95H} expression enhances deposition of UPF1, UPF2, UPF3B in *EZH2*CCWG-3xMS2 transcripts compared to *EZH2*AAWG-3xMS2 (Fig. 4C,D). These enhancements were not observed in K562(DOX)SRSF2^{P95H} cells without DOX treatment. These results clearly pointed out that SRSF2^{Mut}-regulated augmented AS-NMD activity is dependent on sequence-specific binding to *EZH2* PE RNA. Note that we previously showed that SRSF2^{Mut} can directly interact with several spliceosome components, including U1 snRNP and U2 snRNP, as well as EJC factors (Rahman et al. 2020b), which further support the observed results here. In contrast, we did not observe any enhancements of RNPs deposition for SRSF2^{WT} expression (upon DOX treatment) in *EZH2*CCWG-3xMS2 transcripts compared to *EZH2*AAWG-3xMS2 (Fig. 4C,D; Supplemental Fig. S4A,B). This is consistent with our expectation due to the lack of preferred binding motifs of SRSF2^{WT} in *EZH2*CCWG-3xMS2. Note that from these experiments, we cannot compare the relative NMD-inducing efficiency between SRSF2^{Mut} and SRSF2^{WT}, because PE included AS-NMD mRNA of *EZH2* is likely to be generated only in cells expressing SRSF2^{Mut}. However, previously using a reporter of human β-globin (*HBB*) with three constitutive exons and an NMD-inducing nonsense mutation, we showed that SRSF2^{Mut} has a stronger NMD-inducing activity than SRSF2^{WT} (Rahman et al. 2020b).

Taken together, our data propose that sequence-specific binding of SRSF2^{Mut} into *EZH2* PE enhances spliceosome assembly in the flanking splice sites to promote exon inclusion, which is followed by enhanced EJC deposition and subsequent recruitment of NMD factors to facilitate AS-NMD (Fig. 5).

Screening of antisense oligonucleotides to modulate aberrant splicing of EZH2 *poison exon using minigene reporter model*

In the past decade, several pharmacological small-molecule compounds were employed to modulate aberrant splicing in cancer (Lee and Abdel-Wahab 2016; Seiler et al. 2018; Liu et al. 2024). Although a few progressed to clinical trials, they were terminated due to off-target effects (Eskens et al. 2013; Hong et al. 2014) or appeared ineffective (Steensma et al. 2021). Therefore, we undertook a gene-specific targeted approach to correct aberrant splicing of cancer-driver gene(s). We chose antisense pharmacology. Antisense oligonucleotides (ASO) are short synthetic single-stranded nucleic acid molecules that are usually designed to bind to complementary sequences on a target RNA (Rigo et al. 2012; Havens and Hastings 2016). ASO may inhibit the binding of splicing factor(s) or RNA-binding protein(s) or generate steric hindrance to interfere with spliceosome assembly, resulting in differential alternative splicing outcomes. The efficacy of ASO depends on multiple factors (Rigo et al. 2012; Havens and Hastings 2016), such as target site or sequence, binding affinity, cellular delivery, potency, resistance to nuclease, stability, etc. Based on our detail mechanistic characterization of *EZH2* splicing as described above (Fig. 5), we designed four ASOs: ASO1 targeting the flanking 3′ splice site of the PE; ASO2 targeting the SRSF2^{Mut} binding site spanning motif 1 in the PE; ASO3 targeting the SRSF2^{Mut} binding sites spanning both motifs 2 and 3

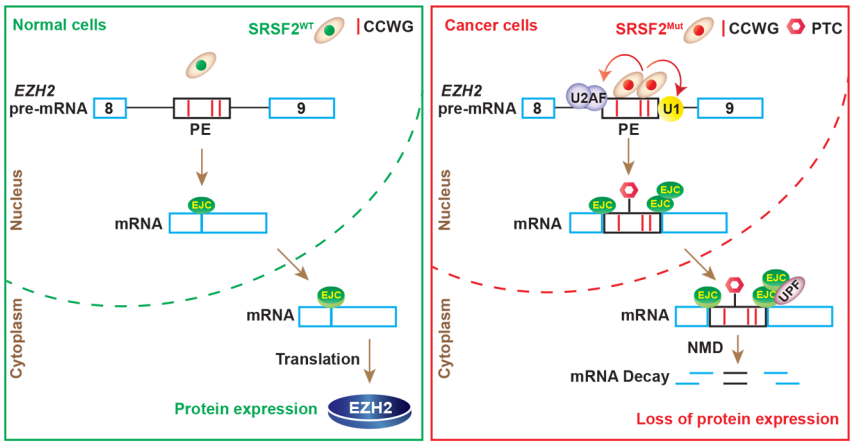

Figure 5. RNA metabolism of *EZH2* in normal and SRSF2 mutated cancer cells. Diagram illustrating how oncogenic mutation at Pro95 of SRSF2 (SRSF2^{Mut}) promotes aberrant AS-NMD of *EZH2*. In normal cells, the lack of the binding motif of the wild-type SRSF2 (SRSF2^{WT}) in the PE results in exon exclusion, producing a productive mRNA that is translated into a functional EZH2 protein. In SRSF2 mutated cancer cells, SRSF2^{Mut} binds to its preferred motifs (CCWG) in the *EZH2* PE, interacts with key spliceosome components, and promotes aberrant inclusion of the PE comprising a PTC. In addition to altering splicing, SRSF2^{Mut} further elicits degradation of *EZH2* mRNA via NMD through dynamic interactions with several EJC proteins and NMD factors, leading to loss of EZH2 protein expression and function. (PE) Poison exon, (PTC) premature termination codon.

in the PE; and ASO4 targeting the flanking 5′ splice site of the PE, respectively (Fig. 6A). We designed ASOs with two different types of base modifications. The first modification was a uniform phosphorothioate backbone and methoxyethyl at the 2′ ribose position (MOE). The second modification was locked nucleic acid (LNA) modification, where a methylene bridge was introduced linking the 2′ oxygen to the 4′ carbon of the pentose ring. These kinds of modifications were previously described to enhance RNA binding affinity and improve resistance to both nucleases- and RNase H-mediated cleavage of the target RNA (Rigo et al. 2012; Havens and Hastings 2016; Nomakuchi et al. 2016; Ma et al. 2022). We set out our initial screening of ASOs for three different concentrations at lower nanomolar ranges (50, 75, and 100 nM). We first tested ASOs targeting the minigene model. We transfected *EZH2*CCWG (native) minigene reporter and MOE ASOs (50, 75, and 100 nM) into K562(DOX)SRSF2^{P95H} cells treated with DOX. As a control, we used no ASO treatment mock control (CTRL). We isolated RNA after 48 h of transfection and quantified *EZH2*CCWG minigene reporter-specific poison exon inclusion using RT-PCR. In our screening, among the four ASOs, we found ASO2 significantly reduced the poison exon inclusion in *EZH2*CCWG minigene in all tested concentrations, with a better efficiency for a higher concentration (Fig. 6B; Supplemental Fig. S5A,C). We also used three additional control MOE ASOs targeting unrelated genes, *HBB*, *MECP2*, and *MUSK*, respectively (Supplemental Fig. S6). These ASOs showed no effect on *EZH2* poison exon inclusion at any of the tested concentrations (50, 75, and 100 nM); therefore, they rule out any experimental artifacts. We then repeated the experiment with LNA ASOs and observed similar results to those of MOE ASOs (Fig. 6C; Supplemental Fig. S5B,D). We also performed these experiments in HeLa(DOX)SRSF2^{P95H} cells treated with DOX (Supplemental Fig. S7). We observed similar results to those of K562(DOX)SRSF2^{P95H}. These results suggest that ASOs designed with two different types of chemical modifications possibly function via the same mechanism of action and are not affected by cell types.

Modulation of EZH2 *poison exon splicing using antisense oligonucleotides in the SRSF2^{MUT} cancer model*

We next tested the effects of ASOs to correct aberrant splicing of endogenous *EZH2* in SRSF2 mutated cancer cells. Although aberrant poison exon inclusion of *EZH2* was consistently identified in cancer patients with mutated SRSF2, both in RNA-seq data and RT-PCR validation, the efficiency of poison exon inclusion was variable in model cell lines across different studies (Kim et al. 2015; Zhang et al. 2015; Liang et al. 2018; Yoshimi et al. 2019; Rahman et al. 2020b). This disparity could be potentially due to the heterogeneous genetic background in cancer patients compared to engineered cell lines. Therefore, we sought a cell line originating from a cancer patient with an inherent SRSF2 mutation. We finally selected the K052 cell line, originated from a leukemia patient with an inherent SRSF2^{P95H} mutation (as described in Fig. 1). Similar to the minigene reporter, we observed that ASO2 (both MOE and LNA) significantly suppressed poison exon inclusion of endogenous *EZH2* (Fig. 6D,E) and restored EZH2 protein expression in K052 (Fig. 6F,G). To determine whether the extent of ASO2-mediated suppression of *EZH2* poison exon inclusion and restoration of EZH2 protein expression can be titrated, we tested ASO2 (both MOE and LNA) for a dose-response experiment. We transfected ASO2 at increasing concentrations (10, 50, 100, 150, and 200 nM) and harvested cells for both RNA and protein isolation after 48 h of the transfection. We indeed found a dose-dependent effect on splicing correction (Fig. 6H,I) and concomitant EZH2 protein expression (Fig. 6J,K). These results show the reproducibility and reliability of our experimental screenings (both minigene and endogenous gene) and proof of concept.

Evaluating the on-target specificity of ASO2 in the SRSF2^{MUT} cancer model

We next evaluated the on-target specificity of our lead ASO (ASO2) in K052 cells. To this end, we checked the splicing profile of several other reported altered splicing events promoted by SRSF2^{Mut}, which have been consistently identified in multiple studies. We included additional 11 targets, including *ARMC10*, *ATF2*, *CDC45*, *CDK5RAP2*, *CRAT*, *DGUOK*, *WDR45*, *INTS3*, *MELK*, *SLC25A26*, and *PFKM* (Kim et al. 2015; Zhang et al. 2015; Yoshimi et al. 2019; Rahman et al. 2020b). We also included K052^{WT} (SRSF2^{WT}) as a control to check whether the effect of ASO2 is specific to cancer cells. We found a consistent differential alternative splicing pattern in K052 cells compared to K052^{WT} cells in all 11 targets (Supplemental Fig. S8). Since MOE and LNA ASOs showed consistent results, we included only LNA ASOs for all downstream experiments. Upon treatment of LNA ASO2 in K052 cells, we could not observe any significant changes in alternative splicing in any of the targets, except *EZH2* (Supplemental Fig. S8). These data highlight the on-target specificity of ASO2 for SRSF2 mutated cancer cells.

ASO2 enhances methylation of histone H3 at lysine 27 to restore EZH2-mediated chromatin regulation in the SRSF2^{MUT} cancer model

We next seek to determine whether ASO2-mediated restoration of EZH2 protein expression rescues EZH2 function. As noted earlier, EZH2 catalyzes methylation of histone H3 at lysine 27 (H3K27me3). We therefore analyzed protein levels of histone H3 and H3K27me3 in K052 cells treated with or without LNA ASO2. We found that the overall expression levels of histone H3 remained similar; however, H3K27me3 levels increased significantly upon ASO2 treatment (Fig. 7A), suggesting that ASO2 could restore EZH2-mediated chromatin regulation. Interestingly, treating K052 with an EZH2 inhibitor (EZH2i) alone did not affect EZH2 expression or H3K27 methylation. However, simultaneous treatment with

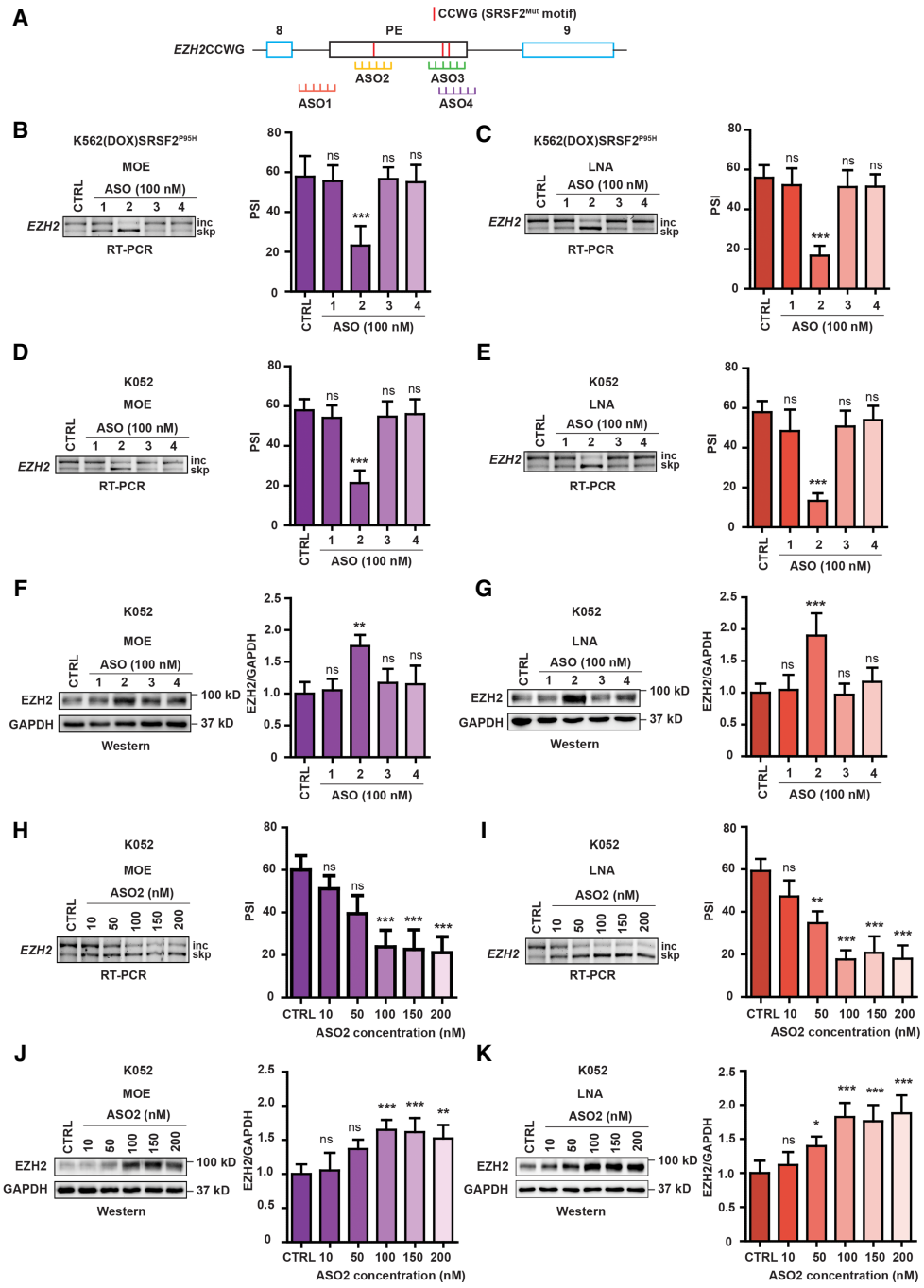

Figure 6. ASO-mediated correction of aberrant poison exon inclusion in *EZH2* in SRSF2 mutated blood cancer. (*A*) Diagram (not to scale) of *EZH2*CCWG (native) minigene reporter and schematics of ASOs and their target binding sites. (*B*,*C*, *left*) Representative RT-PCR gel showing *EZH2* minigene reporter-specific poison exon inclusion (inc) and skipping (skp) of transfected K562(DOX)SRSF2^{P95H} cells in the presence of DOX and treated with 100 nM MOE (*B*) or LNA (*C*) ASOs targeting *EZH2*. (*Right*) Quantification of *EZH2*CCWG minigene reporter-specific poison exon inclusion as percent spliced-in (PSI) is shown by a bar graph. (*D*,*E*, *left*) Representative RT-PCR gel showing endogenous *EZH2* poison exon splicing of K052 cells transfected with 100 nM MOE (*D*) or LNA ASOs (*E*). (*Right*) Quantification of endogenous *EZH2* poison exon inclusion as PSI is shown by a bar graph. (*F*,*G*, *left*) Representative western blotting of EZH2 protein expression of K052 cells transfected with 100 nM MOE (*F*) or LNA ASOs (*G*). GAPDH was used as an internal control. (*Right*) Quantification of relative EZH2 protein expression is shown by a bar graph. (*H*,*I*, *left*) Representative RT-PCR gel showing endogenous *EZH2* poison exon splicing of K052 cells transfected with the indicated doses of MOE (*H*) or LNA ASO2 (*I*). (*Right*) Quantification of endogenous *EZH2* poison exon inclusion as PSI is shown by a bar graph. (*J*,*K*, *left*) Representative western blotting of EZH2 protein expression in K052 cells transfected with the indicated doses of MOE (*J*) or LNA ASO2 (*K*). GAPDH was used as an internal control. (*Right*) Quantification of relative EZH2 protein expression is shown by a bar graph. CTRL: no ASO treatment mock control. All bar graphs (mean ± SD, $n = 3$). (*) $P < 0.05$, (**) $P < 0.01$, (***) $P < 0.001$, (ns) not significant, *t*-test.

both ASO2 and EZH2i, the ASO2-mediated increase in H3K27me3 was attenuated, suggesting that enhanced methylation of histone H3K27 was directly correlated with the restored expression and catalytic function of EZH2 protein.

ASO2 modulates cell viability, cell cycle kinetics, and apoptosis in the SRSF2^{MUT} cancer model

It was previously shown in a murine model that a heterozygous Pro95 mutation in SRSF2 develops MDS with

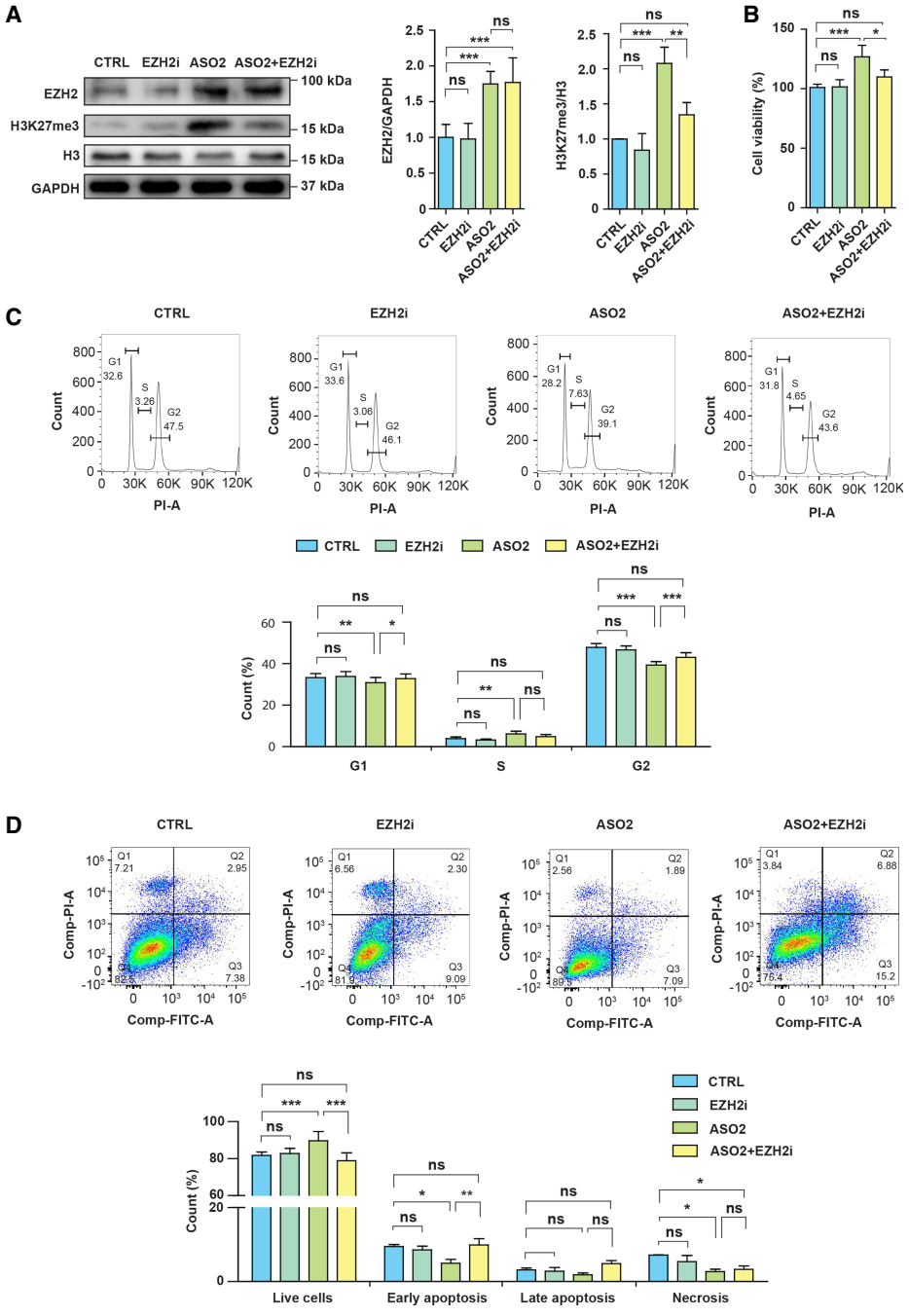

Figure 7. *EZH2* targeting ASO modulates Histone H3K27 methylation, cell viability, cell cycle kinetics, and apoptosis. (*A*, *left*) Western blotting of K052 cells treated with an *EZH2* inhibitor (EZH2i), 100 nM LNA ASO2 targeting *EZH2*, or both simultaneously. CTRL indicates no-treatment control. (*Right*) Quantification of relative protein expression of EZH2 (EZH2/GAPDH) and H3K27me3 (H3K27me3/H3) is shown by bar graphs. (*B*) The XTT cell viability assay of K052 after 5 days with the indicated treatments. (*C*) Cell cycle analysis (*top*) and relative quantification (*bottom*) of K052 with indicated treatments. (*D*) Apoptosis analysis (*top*) and relative quantification (*bottom*) of K052 with indicated treatments. Bar graphs (mean ± SD, $n = 3$). (*) $P < 0.05$, (**) $P < 0.01$, (***) $P < 0.001$, (ns) not significant, two-way ANOVA.

impaired hematopoietic differentiation, altered cell cycle kinetics, and increased apoptosis, resulting in peripheral cytopenia and morphologic dysplasia (Kim et al. 2015). It was further shown that restoring EZH2 expression using a cDNA partially rescues hematopoiesis in *Srsf2* mutant cells (Kim et al. 2015). We therefore tested the effects of LNA ASO2 in rescuing defective hematopoiesis in K052 cells. The XTT cell viability assay revealed that K052 cells treated with 100 nM of LNA ASO2 showed no significant changes on cell viability up to 3 days compared to non-treated cells. However, after 5 days, cell viability was increased for LNA ASO2-treated cells (Fig. 7B). We next followed up cell cycle kinetics using flow cytometry. We found that LNA ASO2 treatment reduced the percentage of cells in both G1 and G2 phases, with a concomitant increase in S phase, showing a preferential progress to cell proliferation (Fig. 7C). In addition, LNA ASO2 treatment reduced early apoptosis and necrosis in K052 (Fig. 7D). Again, addition of EZH2 inhibitor (EZH2i) alone had no measurable effect on cell viability, cell cycle kinetics, or apoptosis. It is important to note that mutations in SRSF2 affect the splicing of several genes linked to tumorigenesis (such as *EZH2*, *INTS3*, and *CLK3*); therefore, correcting the splicing error in *EZH2* alone showed a partial effect in cellular properties. However, correcting all of the tumorigenic targets simultaneously will hopefully exert significant rescue of hematopoiesis and anticancer effects. Furthermore, compared to K052 cells, the effect of ASO may be more effective in treating hematopoietic stem cells over a longer period with combinatorial treatments, and will be an important consideration for therapeutic development. Taken together, antisense-mediated splicing correction shows promising potential as a proof of concept for clinical development. Our future studies will be focused on evaluating the efficacy of our lead ASO in preclinical animal models in vivo and in patient-derived samples, as well as the combinatorial treatment of multiple ASOs targeting multiple genes simultaneously.

Discussion

Since the discovery of recurrent oncogenic mutations in splicing factors, mutations in SRSF2 have been widely studied in hematologic malignancies. Although significant efforts have been employed to identify aberrantly regulated genes, affected pathways, and mechanistic features, the targeted therapeutic development to correct aberrant splicing in SRSF2 mutated cancer has remained limited and ineffective to date. To push the boundary of this underexplored area, we here develop a proof of principle to restore the expression of crucial proteins degraded by AS-NMD and linked to tumorigenesis in SRSF2 mutated cancer through an efficient and gene-specific targeted strategy. We scrutinized the poison exon-mediated AS-NMD event in *EZH2*, a crucial epigenetic regulator frequently altered in AML and other cancers (Guglielmelli et al. 2011; Tan et al. 2014; Kim et al. 2015; Masaki et al. 2019; Sakhdari et al. 2019; Yoshimi et al. 2019; Rahman et al. 2020b; Grimm et al. 2021). Our strategy using antisense oligonucleotide pharmacology efficiently corrects aberrant AS-NMD, restores the expression of EZH2 protein, rescues EZH2-mediated chromatin regulation, and partially improves hematopoiesis and cellular properties.

Although screening of ASOs often exploits random ASOs walking through an entire alternative exon or flanking intronic sequences, we chose to target splicing regulatory regions following precise mechanistic characterization, so that we can develop ASOs with a clear understanding of their mode of action and on-target specificity. Our mechanistic characterization identified three potential regulatory regions for designing ASOs: ESE motifs in the PE to block the binding of $SRSF2^{Mut}$; flanking 3′ splice site to interfere with the binding of U2AF proteins (U2AF35 and U2AF65); and flanking 5′ splice site to interfere with the binding of U1 snRNP. Therefore, we designed four ASOs targeting these three regions. Among the four, the ASO2 targeting motif 1 site efficiently suppressed PE inclusion and restored EZH2 protein expression. This is in agreement with our mechanistic observation, where motif 1 appeared as a crucial determinant of PE inclusion. To our expectation, ASO3 likely failed as we found that binding motifs 2 and 3 are not sufficient and have minimal additive effects. We speculate that 15-mer ASO1 was not enough to block the binding of U2AF65 and U2AF35 or lacked base-pairing affinity to the 3′ splice site. Similarly, ASO4 might fail due to a lack of base-pairing affinity. Designing more ASOs surrounding 3′ and 5′ splice sites may identify efficient ASOs. We exploited two different types of base modifications (MOE-PS and LNA) to enhance binding affinity and stability, but both appeared similarly efficient. Therefore, to improve binding affinity, we probably have to consider the base composition and melting temperature (T_m), rather than chemistries.

As noted earlier, in SRSF2 mutated cancer, only a handful of aberrantly spliced targets were identified and validated with a proven link to tumorigenesis (such as *EZH2*, *INTS3*, and *CLK3*). ASO correcting one gene will show partial rescue and improvement and therefore a limitation for cancer therapy compared to monogenic genetic diseases. To address this shortcoming, the combinatorial treatment of ASOs correcting multiple genes will be more beneficial. Although the focus of this study was to develop a therapeutic proof of concept based on mechanistic characterization, our future research will develop ASOs for combinatorial therapy targeting multiple genes and will test them in preclinical animal models in vivo and hopefully progress to clinical development.

Materials and methods

Patient samples

All human-related studies were approved by the Institutional Review Boards and conducted in accordance with the Declaration of Helsinki protocol. AML patient

samples were obtained from de-identified patients at Memorial Sloan Kettering Cancer Center.

Minigene reporters

The native *EZH2* minigene reporter (*EZH2*CCWG) was kindly shared by Dr. Robert Bradley (Fred Hutchinson Cancer Center) (Kim et al. 2015). We generated different versions of the *EZH2* minigene reporter using site-directed mutagenesis. We confirmed the accuracy of the reporters by sequencing the entire inserts.

cDNA constructs

T7-SRSF2^{WT}, T7-SRSF2^{P95H}, MS2, MS2-T7-SRSF2^{WT}, and MS2-T7-SRSF2^{P95H} cDNA constructs were previously described (Rahman et al. 2020b). We generated DOX-inducible FLAG-tagged SRSF2^{WT} and SRSF2^{P95H} cDNA constructs in pInducer20 (Addgene) (Meerbrey et al. 2011).

Cell culture

The sources and information of different cell lines are summarized in Supplemental Table S1. K562, K562^{Mut}, MOLM-13, SET2, K052, and K052^{WT} cells were cultured in RPMI-1640 medium, whereas HeLa and 293T cells were cultured in DMEM media. All cells were grown with respective medium supplemented with 10% fetal bovine serum (FBS) and maintained in an incubator at 37°C with 5% CO_2. K562(DOX)SRSF2$^{WT\ or\ P95H}$ or HeLa(DOX)SRSF2$^{WT\ or\ P95H}$ cells were stimulated by 1 µg/mL doxycycline (DOX).

Cell transfection

Cells were transfected with Lipofectamine 3000 reagent (Invitrogen) according to the manufacturer's instructions.

Splicing analysis using reverse transcription PCR (RT-PCR)

Total RNA was extracted 48 h after transfection of minigene reporter (unless otherwise mentioned) using TRIzol reagent, followed by DNase treatment. Reverse transcription reaction was performed with ImProm-II reverse transcriptase (Promega). During cDNA synthesis, we used oligo-dT reverse primer to check endogenous gene splicing. In contrast, we used a minigene reporter-specific reverse primer during cDNA synthesis to check minigene reporter-specific splicing events. PCR reaction was performed by Phusion high-fidelity PCR master mix with HF buffer (New England Biolabs M0531L). The sequences of primers are listed in Supplemental Table S2.

Western blotting

Western blotting was conducted as described previously (Rahman et al. 2020b). The list of antibodies used is in Supplemental Table S3.

MS2-mediated purification of mRNA-protein complexes

K562(DOX)SRSF2$^{WT\ or\ P95H}$ cells were stimulated by 1 µg/mL doxycycline (DOX) in 15 cm plates. After overnight culture, the cells were transfected with *EZH2* CCWG-3xMS2 or *EZH2*AAWG-3xMS2 reporter using Lipofectamine 3000. The MS2-mediated purification of mRNA–protein complexes was conducted as described previously (Rahman et al. 2020b). Purified proteins were resolved by western blotting, and purified reporter-specific RNAs were amplified by RT-PCR using primers targeting a common region spanning all transcripts.

Antisense oligonucleotides (ASO)-mediated splicing correction

We synthesized ASOs from Integrated DNA Technologies (IDT). The sequences of ASOs are listed in Supplemental Table S4. We transfected ASOs using Lipofectamine 3000 reagent (Invitrogen).

EZH2 inhibitor

The EZH2 inhibitor, EPZ-6438 (Tazemetostat), was purchased from SelleckChem (S7128) and used according to the manufacturer's instructions.

Analyses of cell viability and cellular phenotypes

We tested the effects of ASOs or EZH2 inhibitor on cell viability and cell cycle kinetics of K052. For cell viability, we evaluated the percentage of K052 cell survival by the XTT cell viability assay (Thermo Fisher Scientific X12223) and counted cell numbers by QuadCount automated cell counter (E7500) after ASO treatment.

Flow cytometry analysis

K052 cells treated with ASO2 or EZH2 inhibitor or non-treated cells were stained by propidium iodide (PI) (V13242, Thermo Fisher Scientific) for cell cycle and by Annexin V and PI for apoptosis, and then evaluated using BD LSRFortessa-flow analyses according to the manufacturer's instructions. The data were evaluated by FlowJo software, and the results were compared to the control group.

Quantification and statistical analysis

Densitometric analysis of RT-PCR or western blotting was done by ImageJ software. Statistical analysis was performed either by *t*-test or ANOVA. Data are presented as mean and standard deviation, indicated by error bars, and all plots were generated using GraphPad Prism software.

Data availability

The data underlying this study are available here and in the Supplemental Material.

Competing interest statement

M.A.R., M.R.I., and P.N. are inventors on a patent application related to this study. O.A.-W. is one of the founders and scientific advisors of Codify Therapeutics; he holds equity and receives research funding from this company. O.A.-W. has served as a consultant for Amphista Therapeutics and MagnetBio and is on the scientific advisory boards of Envisagenics, Inc., and Harmonic Discovery, Inc. O.A.-W. received research funding from Nurix Therapeutics, Minovia Therapeutics, and LOXO Oncology unrelated to this study. A.R.K. discloses the following commercial associations, unrelated to this study: Stoke Therapeutics (Cofounder and Director); scientific advisory boards of Skyhawk Therapeutics, Envisagenics, and Autoimmunity BioSolutions; and consultant for Biogen, SEED Therapeutics, Crucible Therapeutics, Cajal Neuroscience, and Collage Bio.

Acknowledgments

We are grateful to Robert Bradley (Fred Hutchinson Cancer Center) for sharing the *EZH2* minigene. M.A.R. was supported by the National Institute of General Medical Sciences (NIGMS) of the National Institutes of Health (R35GM154991 and P20GM152281), Edward P. Evans Foundation, and Winthrop P. Rockefeller Cancer Institute.

Author contributions: M.A.R. conceived the project and supervised the study. M.A.R., A.R.K., M.R.I., and P.N. designed the experiments. M.R.I. and P.N. performed all the experiments with the help of N.M., S.A.H., M.M.H., S.K., and I.J.M. O.A.-W. provided AML patient RNA samples and human leukemia cell lines. A.R.K. provided MS2-tagged cDNA constructs. W.B.D. and P.T. provided the K052^{WT} cell line. O.A.-W. and A.R.K. helped in critical data interpretation and shared analytical protocols. M.R.I., P.N., and M.A.R. wrote the original draft of the manuscript. M.A.R., O.A.-W., and A.R.K. finalized the manuscript. All authors approved the final version of the manuscript.

References

Bailey TL, Boden M, Buske FA, Frith M, Grant CE, Clementi L, Ren J, Li WW, Noble WS. 2009. MEME SUITE: tools for motif discovery and searching. *Nucleic Acids Res* **37:** W202–W208. doi:10.1093/nar/gkp335

Black DL. 2003. Mechanisms of alternative pre-messenger RNA splicing. *Annu Rev Biochem* **72:** 291–336. doi:10.1146/annurev.biochem.72.121801.161720

Bradley RK, Anczuków O. 2023. RNA splicing dysregulation and the hallmarks of cancer. *Nat Rev Cancer* **23:** 135–155. doi:10.1038/s41568-022-00541-7

Colombo M, Karousis ED, Bourquin J, Bruggmann R, Mühlemann O. 2017. Transcriptome-wide identification of NMD-targeted human mRNAs reveals extensive redundancy between SMG6- and SMG7-mediated degradation pathways. *RNA* **23:** 189–201. doi:10.1261/rna.059055.116

Darman RB, Seiler M, Agrawal AA, Lim KH, Peng S, Aird D, Bailey SL, Bhavsar EB, Chan B, Colla S, et al. 2015. Cancer-associated SF3B1 hotspot mutations induce cryptic 3′ splice site selection through use of a different branch point. *Cell Rep* **13:** 1033–1045. doi:10.1016/j.celrep.2015.09.053

Daver N, Wei AH, Pollyea DA, Fathi AT, Vyas P, DiNardo CD. 2020. New directions for emerging therapies in acute myeloid leukemia: the next chapter. *Blood Cancer J* **10:** 107. doi:10.1038/s41408-020-00376-1

Eskens FALM, Ramos FJ, Burger H, O'Brien JP, Piera A, de Jonge MJA, Mizui Y, Wiemer EAC, Carreras MJ, Baselga J, et al. 2013. Phase I pharmacokinetic and pharmacodynamic study of the first-in-class spliceosome inhibitor E7107 in patients with advanced solid tumors. *Clin Cancer Res* **19:** 6296–6304. doi:10.1158/1078-0432.CCR-13-0485

Feng H, Bao S, Rahman MA, Weyn-Vanhentenryck SM, Khan A, Wong J, Shah A, Flynn ED, Krainer AR, Zhang C. 2019. Modeling RNA-binding protein specificity in vivo by precisely registering protein-RNA crosslink sites. *Mol Cell* **74:** 1189–1204.e6. doi:10.1016/j.molcel.2019.02.002

Graubert TA, Shen D, Ding L, Okeyo-Owuor T, Lunn CL, Shao J, Krysiak K, Harris CC, Koboldt DC, Larson DE, et al. 2011. Recurrent mutations in the U2AF1 splicing factor in myelodysplastic syndromes. *Nat Genet* **44:** 53–57. doi:10.1038/ng.1031

Grimm J, Jentzsch M, Bill M, Backhaus D, Brauer D, Küpper J, Schulz J, Franke G, Vucinic V, Niederwieser D, et al. 2021. Clinical implications of *SRSF2* mutations in AML patients undergoing allogeneic stem cell transplantation. *Am J Hematol* **96:** 1287–1294. doi:10.1002/ajh.26298

Guglielmelli P, Biamonte F, Score J, Hidalgo-Curtis C, Cervantes F, Maffioli M, Fanelli T, Ernst T, Winkelman N, Jones AV, et al. 2011. EZH2 mutational status predicts poor survival in myelofibrosis. *Blood* **118:** 5227–5234. doi:10.1182/blood-2011-06-363424

Havens MA, Hastings ML. 2016. Splice-switching antisense oligonucleotides as therapeutic drugs. *Nucleic Acids Res* **44:** 6549–6563. doi:10.1093/nar/gkw533

Hong DS, Kurzrock R, Naing A, Wheler JJ, Falchook GS, Schiffman JS, Faulkner N, Pilat MJ, O'Brien J, LoRusso P. 2014. A phase I, open-label, single-arm, dose-escalation study of E7107, a precursor messenger ribonucleic acid (pre-mRNA) splicesome inhibitor administered intravenously on days 1 and 8 every 21 days to patients with solid tumors. *Invest New Drugs* **32:** 436–444. doi:10.1007/s10637-013-0046-5

Ilagan JO, Ramakrishnan A, Hayes B, Murphy ME, Zebari AS, Bradley P, Bradley RK. 2015. *U2AF1* mutations alter splice site recognition in hematological malignancies. *Genome Res* **25:** 14–26. doi:10.1101/gr.181016.114

Inoue D, Chew G-L, Liu B, Michel BC, Pangallo J, D'Avino AR, Hitchman T, North K, Lee SC-W, Bitner L, et al. 2019. Spliceosomal disruption of the non-canonical BAF complex in cancer. *Nature* **574:** 432–436. doi:10.1038/s41586-019-1646-9

Kim E, Ilagan JO, Liang Y, Daubner GM, Lee SC-W, Ramakrishnan A, Li Y, Chung YR, Micol J-B, Murphy ME, et al. 2015. SRSF2 mutations contribute to myelodysplasia by mutant-specific effects on exon recognition. *Cancer Cell* **27:** 617–630. doi:10.1016/j.ccell.2015.04.006

Kim WJ, Crosse EI, De Neef E, Etxeberria I, Sabio EY, Wang E, Bewersdorf JP, Lin K-T, Lu SX, Belleville A, et al. 2025. Mis-splicing-derived neoantigens and cognate TCRs in splicing factor mutant leukemias. *Cell* **188:** 3422–3440.e24. doi:10.1016/j.cell.2025.03.047

Komeno Y, Huang Y-J, Qiu J, Lin L, Xu Y, Zhou Y, Chen L, Monterroza DD, Li H, DeKelver RC, et al. 2015. SRSF2 is essential for hematopoiesis, and its myelodysplastic syndrome-related mutations dysregulate alternative pre-mRNA splicing. *Mol Cell Biol* **35:** 3071–3082. doi:10.1128/MCB.00202-15

Kurosaki T, Popp MW, Maquat LE. 2019. Quality and quantity control of gene expression by nonsense-mediated mRNA decay. *Nat Rev Mol Cell Biol* **20:** 406–420. doi:10.1038/s41580-019-0126-2

Lee SC-W, Abdel-Wahab O. 2016. Therapeutic targeting of splicing in cancer. *Nat Med* **22:** 976–986. doi:10.1038/nm.4165

Liang Y, Tebaldi T, Rejeski K, Joshi P, Stefani G, Taylor A, Song Y, Vasic R, Maziarz J, Balasubramanian K, et al. 2018. SRSF2 mutations drive oncogenesis by activating a global program of aberrant alternative splicing in hematopoietic cells. *Leukemia* **32:** 2659–2671. doi:10.1038/s41375-018-0152-7

Licatalosi DD, Darnell RB. 2006. Splicing regulation in neurologic disease. *Neuron* **52:** 93–101. doi:10.1016/j.neuron.2006.09.017

Liu ZS, Sinha S, Bannister M, Song A, Arriaga-Gomez E, McKeeken AJ, Bonner EA, Hanson BK, Sarchi M, Takashima K, et al. 2024. R-loop accumulation in spliceosome mutant leukemias confers sensitivity to PARP1 inhibition by triggering transcription–replication conflicts. *Cancer Res* **84:** 577–597. doi:10.1158/0008-5472.CAN-23-3239

Lykke-Andersen S, Jensen TH. 2015. Nonsense-mediated mRNA decay: an intricate machinery that shapes transcriptomes. *Nat Rev Mol Cell Biol* **16:** 665–677. doi:10.1038/nrm4063

Ma WK, Voss DM, Scharner J, Costa ASH, Lin K-T, Jeon HY, Wilkinson JE, Jackson M, Rigo F, Bennett CF, et al. 2022. ASO-based PKM splice-switching therapy inhibits hepatocellular carcinoma growth. *Cancer Res* **82:** 900–915. doi:10.1158/0008-5472.CAN-20-0948

Masaki S, Ikeda S, Hata A, Shiozawa Y, Kon A, Ogawa S, Suzuki K, Hakuno F, Takahashi S-I, Kataoka N. 2019. Myelodysplastic syndrome-associated SRSF2 mutations cause splicing changes by altering binding motif sequences. *Front Genet* **10:** 338. doi:10.3389/fgene.2019.00338

Meerbrey KL, Hu G, Kessler JD, Roarty K, Li MZ, Fang JE, Herschkowitz JI, Burrows AE, Ciccia A, Sun T, et al. 2011. The pINDUCER lentiviral toolkit for inducible RNA interference in vitro and in vivo. *Proc Natl Acad Sci* **108:** 3665–3670. doi:10.1073/pnas.1019736108

Nagar P, Islam MR, Rahman MA. 2023. Nonsense-mediated mRNA decay as a mediator of tumorigenesis. *Genes (Basel)* **14:** 357. doi:10.3390/genes14020357

Nasrin F, Rahman MA, Masuda A, Ohe K, Takeda J-I, Ohno K. 2014. HnRNP C, YB-1 and hnRNP L coordinately enhance skipping of human musk exon 10 to generate a wnt-insensitive musk isoform. *Sci Rep* **4:** 6841. doi:10.1038/srep06841

Nasrin F, Nagar P, Islam MR, Heeamoni SA, Hasan MM, Ohno K, Rahman MA. 2025. SRSF6 and SRSF1 coordinately enhance the inclusion of human *MUSK* exon 10 to generate a Wnt-sensitive MuSK isoform. *NAR Mol Med* **2:** ugaf007. doi:10.1093/narmme/ugaf007

Nomakuchi TT, Rigo F, Aznarez I, Krainer AR. 2016. Antisense oligonucleotide–directed inhibition of nonsense-mediated mRNA decay. *Nat Biotechnol* **34:** 164–166. doi:10.1038/nbt.3427

Park S, Brugiolo M, Akerman M, Das S, Urbanski L, Geier A, Kesarwani AK, Fan M, Leclair N, Lin K-T, et al. 2019. Differential functions of splicing factors in mammary transformation and breast cancer metastasis. *Cell Rep* **29:** 2672–2688.e7. doi:10.1016/j.celrep.2019.10.110

Popp MW-L, Maquat LE. 2014. The dharma of nonsense-mediated mRNA decay in mammalian cells. *Mol Cells* **37:** 1–8. doi:10.14348/molcells.2014.2193

Popp MW, Maquat LE. 2018. Nonsense-mediated mRNA decay and cancer. *Curr Opin Genet Dev* **48:** 44–50. doi:10.1016/j.gde.2017.10.007

Rahman MA, Krainer AR, Abdel-Wahab O. 2020a. Snapshot: Splicing alterations in cancer. *Cell* **180:** 208–208.e1. doi:10.1016/j.cell.2019.12.011

Rahman MA, Lin K-T, Bradley RK, Abdel-Wahab O, Krainer AR. 2020b. Recurrent SRSF2 mutations in MDS affect both splicing and NMD. *Genes Dev* **34:** 413–427. doi:10.1101/gad.332270.119

Rigo F, Hua Y, Krainer AR, Bennett CF. 2012. Antisense-based therapy for the treatment of spinal muscular atrophy. *J Cell Biol* **199:** 21–25. doi:10.1083/jcb.201207087

Sakhdari A, Class C, Montalban-Bravo G, Sasaki K, Bueso-Ramos CE, Patel KP, Khoury JD, Kantarjian HM, Garcia-Manero G, Medeiros LJ, et al. 2019. Loss of EZH2 protein expression in myelodysplastic syndrome correlates with EZH2 mutation and portends a worse outcome. *Blood* **134:** 3016. doi:10.1182/blood-2019-131774

Seiler M, Yoshimi A, Darman R, Chan B, Keaney G, Thomas M, Agrawal AA, Caleb B, Csibi A, Sean E, et al. 2018. H3B-8800, an orally available small-molecule splicing modulator, induces lethality in spliceosome-mutant cancers. *Nat Med* **24:** 497–504. doi:10.1038/nm.4493

Steensma DP, Wermke M, Klimek VM, Greenberg PL, Font P, Komrokji RS, Yang J, Brunner AM, Carraway HE, Ades L, et al. 2021. Phase I first-in-human dose escalation study of the oral SF3B1 modulator H3B-8800 in myeloid neoplasms. *Leukemia* **35:** 3542–3550. doi:10.1038/s41375-021-01328-9

Tan J, Yan Y, Wang X, Jiang Y, Xu HE. 2014. EZH2: biology, disease, and structure-based drug discovery. *Acta Pharmacol Sin* **35:** 161–174. doi:10.1038/aps.2013.161

Woodward LA, Mabin JW, Gangras P, Singh G. 2017. The exon junction complex: a lifelong guardian of mRNA fate. *WIREs RNA* **8:** e1411. doi:10.1002/wrna.1411

Yoshida K, Sanada M, Shiraishi Y, Nowak D, Nagata Y, Yamamoto R, Sato Y, Sato-Otsubo A, Kon A, Nagasaki M, et al. 2011. Frequent pathway mutations of splicing machinery in myelodysplasia. *Nature* **478:** 64–69. doi:10.1038/nature10496

Yoshimi A, Lin K-T, Wiseman DH, Rahman MA, Pastore A, Wang B, Lee SC-W, Micol J-B, Zhang XJ, de Botton S, et al. 2019. Coordinated alterations in RNA splicing and epigenetic regulation drive leukaemogenesis. *Nature* **574:** 273–277. doi:10.1038/s41586-019-1618-0

Zhang J, Lieu YK, Ali AM, Penson A, Reggio KS, Rabadan R, Raza A, Mukherjee S, Manley JL. 2015. Disease-associated mutation in *SRSF2* misregulates splicing by altering RNA-binding affinities. *Proc Natl Acad Sci* **112:** E4726–E4734. doi:10.1073/pnas.1514105112

Zhang Q, Ai Y, Abdel-Wahab O. 2024. Molecular impact of mutations in RNA splicing factors in cancer. *Mol Cell* **84:** 3667–3680. doi:10.1016/j.molcel.2024.07.019